Original Article

# The influence of $^{18}$F-fluorodeoxyglucose positron emission tomography/computed tomography on the N- and M-staging and subsequent clinical management of intrahepatic cholangiocarcinoma

**Youpei Lin[1#], Huanhuan Chong[2#], Guohe Song[1#], Chenhao Zhang[1], Liangqing Dong[1], Ling Aye[1], Fei Liang[3], Shuaixi Yang[1], Mengsu Zeng[2], Guangyu Ding[1], Shu Zhang[1], Jieyi Shi[1], Aiwu Ke[1], Xiaoying Wang[1], Jian Zhou[1,4], Jia Fan[1,4], Qiang Gao[1,4]**

[1]Department of Liver Surgery and Transplantation, Liver Cancer Institute, Zhongshan Hospital, and Key Laboratory of Carcinogenesis and Cancer Invasion (Ministry of Education), Fudan University, Shanghai, China; [2]Department of Radiology, Zhongshan Hospital, Fudan University, Shanghai, China; [3]Department of Biostatistics, Zhongshan Hospital, Fudan University, Shanghai, China; [4]Key Laboratory of Medical Epigenetics and Metabolism, Institutes of Biomedical Sciences, Fudan University, Shanghai, China

*Contributions:* (I) Conception and design: Q Gao, J Fan, Y Lin, G Song; (II) Administrative support: J Fan; (III) Provision of study materials or patients: C Zhang, L Dong, L Aye; (IV) Collection and assembly of data: Y Lin, G Song, S Yang, G Ding, S Zhang, J Shi, X Wang; (V) Data analysis and interpretation: H Chong, F Liang, M Zeng, A Ke, J Zhou; (VI) Manuscript writing: All authors; (VII) Final approval of manuscript: All authors.

[#]These authors contributed equally to this work.

*Correspondence to:* Qiang Gao; Jia Fan. Department of Liver Surgery and Transplantation, Liver Cancer Institute, Zhongshan Hospital, Fudan University, 180 Fenglin Road, Shanghai, China. Email: gaoqiang@fudan.edu.cn; fan.jia@zs-hospital.sh.cn.

**Background:** Intrahepatic cholangiocarcinoma (ICC) is a highly metastatic cancer. $^{18}$F-fluorodeoxyglucose positron emission tomography/computed tomography ($^{18}$F-FDG PET/CT) enables sensitive tumor and metastasis detection. Our aim is to evaluate the influence of pre-treatment PET/CT on the N- and M-staging and subsequent clinical management in ICC patients.

**Methods:** Between August 2010 and August 2018, 660 consecutive ICC patients, without prior anti-tumor treatments nor other malignancies, were enrolled. The diagnostic performance of PET/CT on the N- and M-staging was compared with conventional imaging, and the preoperative staging accuracy and treatment re-allocation by PET/CT were retrospectively calculated. Survival difference was compared between patients receiving PET/CT or not after propensity score matching.

**Results:** Patients were divided into group A (n=291) and group B (n=369) according to whether PET/CT was performed. Among 291 patients with both PET/CT and conventional imaging for staging in group A, PET/CT showed significantly higher sensitivity (83.0% *vs.* 70.5%, P=0.001), specificity (88.3% *vs.* 74.9%, P<0.001) and accuracy (86.3% *vs.* 73.2%, P<0.001) than conventional imaging in diagnosing regional lymph node metastasis, as well as higher sensitivity (87.8% *vs.* 67.6%, P<0.001) and accuracy (93.5% *vs.* 89.3%, P=0.023) in diagnosing distant metastasis. Overall, PET/CT improved the accuracy of preoperative staging from 60.1% to 71.8% (P<0.001), and modified clinical treatment strategy in 5.8% (17/291) of ICC patients, with unique roles in different tumor-node-metastasis (TNM) stages. High tumor-to-non-tumor ratio (TNR) predicted poor overall survival [hazard ratio (HR) = 2.17; 95% confidence interval (CI): 1.49–3.15; P<0.001]. Furthermore, patients performing PET/CT had longer overall survival compared with those without PET/CT (HR =0.74; 95% CI: 0.58–0.93; P=0.011) after propensity score matching.

**Conclusions:** PET/CT was valuable for diagnosing regional lymph node metastasis and distant metastasis in ICC patients, and facilitated accurate tumor staging and optimal treatment allocation.

**Keywords:** Intrahepatic cholangiocarcinoma (ICC); staging; positron emission tomography/computed

tomography (PET/CT); clinical management

Submitted Jan 19, 2021. Accepted for publication May 14, 2021.
doi: 10.21037/hbsn-21-25
**View this article at:** https://dx.doi.org/10.21037/hbsn-21-25

## Introduction

Intrahepatic cholangiocarcinoma (ICC) is the second most common primary liver cancer after hepatocellular carcinoma, with increasing incidence and mortality worldwide (1,2). The clinical management of ICC remains challenging due to limited treatment options. Surgical resection is the only potentially curative treatment for selective patients, but postoperative survival is poor and significantly varies across different tumor-node-metastasis (TNM) stages (3). For those with distant metastasis, surgery is not recommended and systemic therapy is needed. Thus, accurate tumor staging and tumor burden estimation are extremely important for optimal treatment allocation in ICC.

$^{18}$F-fluorodeoxyglucose positron emission tomography/computed tomography ($^{18}$F-FDG PET/CT) provides both molecular information of glucose metabolism and precise anatomical location of lesions, which is known for its value in detecting occult metastasis (4), diagnosing early tumor relapse (5), and monitoring treatment effect (6). Hence, PET/CT has been widely used in clinical oncological practice as a supplement to conventional imaging examinations (CIE) including computed tomography (CT) and magnetic resonance imaging (MRI).

Despite that ICC is highly metastatic, the role of PET/CT in ICC has not been well established in clinical practice guidelines, which may limit its application (7-10). Although PET/CT has no obvious advantages over CIE in diagnosing primary tumor of ICC (11), emerging evidence has shown its potential in detecting extrahepatic metastasis (12-14), predicting prognosis (15-17), and refining treatment strategy (18,19). However, those studies always enrolled small cohorts with both intrahepatic and extrahepatic biliary cancers, yielding conflicting results and thus requiring validation in larger cohorts. Meanwhile, little is known about the precise role of PET/CT in different TNM stages of ICC patients and its effect on survival outcomes. Therefore, we conducted this retrospective study in large cohort of ICC patients to compare the diagnostic performance of PET/CT and conventional imaging on the N- and M-staging, and evaluate the influence of PET/CT on subsequent clinical management. We present the following article in accordance with the STARD reporting checklist (available at https://hbsn.amegroups.com/article/view/10.21037/hbsn-21-25/rc).

## Methods

### *Patient selection*

Between August 2010 and August 2018, 660 consecutive patients with pathologically confirmed ICC, and complete clinical and imaging data, without prior anti-tumor treatments nor other malignancies, were retrospectively enrolled (*Figure 1*). All the patients underwent abdominal contrast-enhanced MRI and/or CT, and chest radiography or CT for preoperative evaluation, 291 of whom received PET/CT for pre-treatment staging. The median time between abdominal MRI/CT and PET/CT was 2 days (range, 0–20 days). Detailed imaging examinations were listed in Table S1. The study was conducted in accordance with the Declaration of Helsinki (as revised in 2013). The study was approved by institutional ethics board of Zhongshan Hospital, Fudan University (No. B2020-322) and informed consent was taken from all individual participants.

### *Imaging techniques*

Three PET/CT instruments (GE Discovery VCT 64, GE company, USA; UMI 510, UMI 780, United imaging, China) were performed with routine CT parameters (tube voltage, 120–140 kV; tube current, 140 mA; slice thickness, 3.75 mm; pitch, 0.516; rotating speed, 0.33 s/r; matrix, 512×512; spacing, 1.25 mm) and PET parameters (visual field, 15 cm; 2 min/bed, 6–8 beds/patient). PET data was first attenuated based on CT, then filtered and reconstructed based on ordered subset expectation maximization. Before the injection of $^{18}$F-FDG (3.7–5.6 MBq/kg; Shanghai Atomic Science and Technology Pharmaceutical Co., Ltd., China), patients were required to fast for more than 6 hours (for satisfying serum glucose levels within 7.4 mmol/L). Patients with diabetes needed to keep their serum glucose at

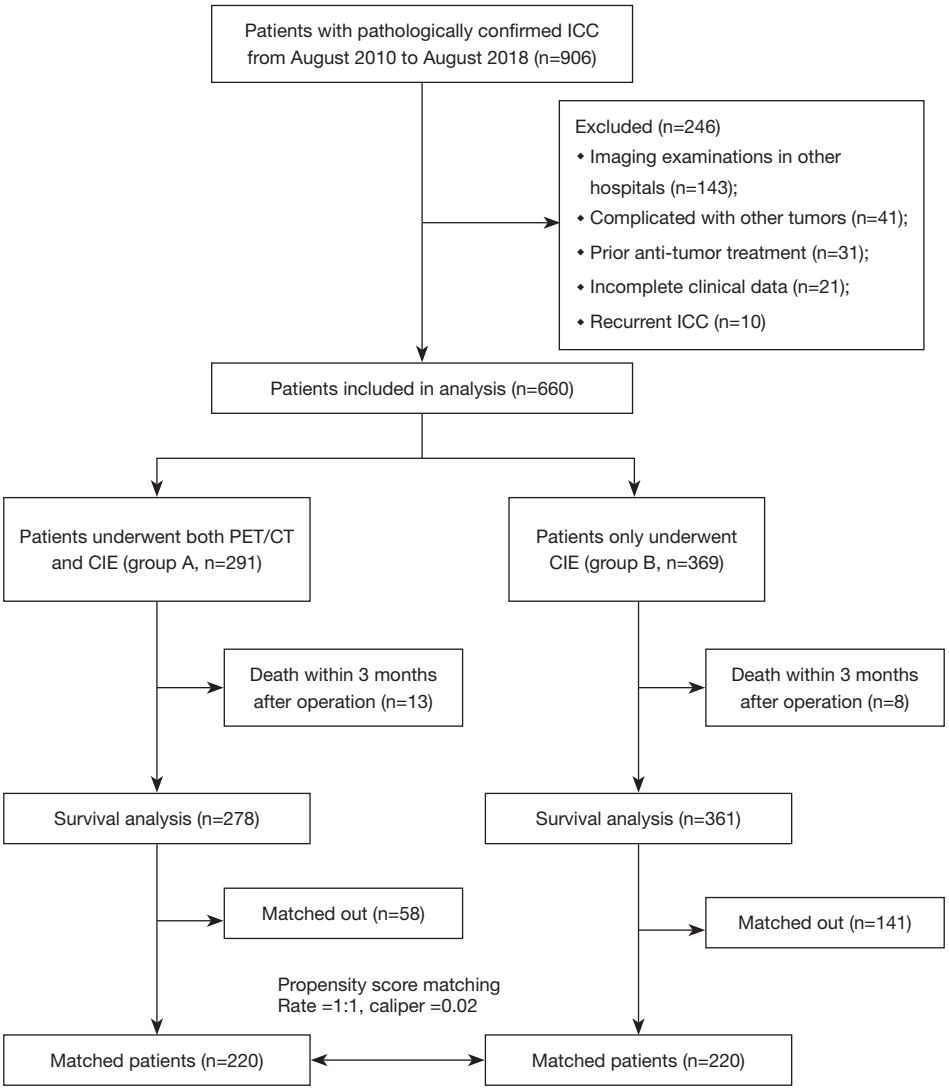


**Figure 1** Flow chart of patient selection. ICC, intrahepatic cholangiocarcinoma; PET/CT, positron emission tomography/computed tomography; CIE, conventional imaging examination.

normal levels 2–3 days before the PET/CT examination. To reduce the non-neoplastic physiological intake of $^{18}$F-FDG, patients were demanded to rest for approximate 60 minutes in the dark room before scanning.

Contrast-enhanced MRI was performed with gadopentetate dimeglumine (Magnevist, Bayer Pharma, Berlin, Germany; 3.0 mL/s) on 1.5 or 3.0 Tesla scanners. Abdominal sequences were as below: transverse fat-suppressed T2-weighted imaging, magnetic resonance (MR) cholangiopancreatography, gradient echo T1-weighted in-phase and opposed-phase imaging, free-breathing diffusion-weighted imaging (b value, 0 and 500 s/mm$^2$), apparent diffusion coefficient mapping, pre-contrast and dynamic contrast-enhanced images (arterial phase 20–30 s; portal venous phase, 60–70 s; delayed phase, 180 s) using three-dimensional T1-weighted volumetric-interpolated breath-hold examination. More parameters were displayed in Table S2.

Several multi-slice CT scanners were implemented with contrast medium (Ultravist 300 mgI/mL, Bayer Healthcare, Berlin, Germany; 1.5 mL/kg and 3.0 mL/s) for detecting liver lesions. The corresponding slice thickness, tube current, peak voltage, pitch, rotation time, field of view, and matrix were 5 mm, 120–200 mA, 120 kV, 0.85–1.0, 0.5 s, 320–380 mm, and 512×512, respectively. Scanning protocols included pre-contrast, arterial, portal venous, and

delay phases.

### *Imaging analysis*

The MRIs, CTs, and chest radiography were independently interpreted by two experienced radiologists, and PET/CT was independently interpreted by two experienced nuclear physicians. These readers were blinded to the pathologic information. A consensus was reached after mutual consultation in cases of discrepancy. As a semi-quantitative indicator of tumor glycolysis in PET/CT, standardized uptake value (SUV) was calculated as activity of imaging agent per unit volume of the lesion divided by injection dose divided by body weight in kilograms. The maximum of SUV was defined as SUVmax, and the SUVmax of normal liver was calculated as the average of 5 regions of interest (ROIs) from different liver segments (12). Tumor-to-non-tumor ratio (TNR) was defined as SUVmax of the tumor divided by SUVmax of the normal liver.

Regional lymph node (LN) metastases were limited at the hilar, periduodenal, and peripancreatic areas, beyond where were defined as distant metastases (9). LNs were interpreted as malignant on CIE if their short-axis diameter exceeded 10 mm (20). In PET/CT, LNs were interpreted as positive for metastasis based on SUVmax beyond 2.5 (21). The interpretation of distant metastases depended on anatomic information and abnormal radiographic findings. By PET/CT, elevated FDG uptake of lesions assisted in determining malignancy or not.

### *Reference standard*

When available, surgical resection or biopsy of LNs and metastatic lesions were used as the standard of reference. For cases without pathological results, we reviewed follow-up imaging and applied the RECIST to determine malignancy when lesions met the criteria of progression (22).

### *Tumor staging and treatment allocation*

Patients were staged according to the 8$^{th}$ edition of American Joint Committee on Cancer (AJCC)-classification system (23). CIE staging was solely based on the preoperative CIE including abdominal contrast-enhanced MRI and/or CT, and chest radiography or CT. PET/CT staging was based on the combination of preoperative PET/CT and CIE. The final staging was based on the combination of pre-treatment imaging, surgery, pathology, and post-treatment follow-up imaging. The accuracy of CIE staging and PET/CT staging was calculated by comparing with the final staging. The modification of treatment allocation was reviewed according to electronic patient records.

### *Propensity score matching (PSM)*

Because PET/CT examination was not randomly assigned to patients, we applied PSM to reduce selection bias and potential confounding factors. Variables that may influence the assignation of PET/CT and clinical outcomes, including age, gender, clinical symptom, carbohydrate antigen 19-9 (CA19-9), carcinoembryonic antigen (CEA), hepatitis B virus (HBV) infection, liver cirrhosis, tumor diameter, tumor number, vascular invasion, regional LN metastasis, and distant metastasis, were comprehensively enrolled in the calculation of the propensity score. The caliper value was set as 0.02 and binary logistic regression was used to generate a propensity score from 0 to 1. Nearest-neighbor matching was used without replacement at a ratio of 1:1.

### *Statistical analysis*

The primary outcome measures were the sensitivity and specificity of PET/CT compared with conventional imaging in diagnosing regional LN metastasis. A total of 280 patients with both PET/CT and conventional imaging were need to detect a 15% difference in sensitivity and specificity at the 0.05 level of significance with 80% power, assuming a 70% sensitivity and 75% specificity of conventional imaging and a regional LN metastasis prevalence rate of 40%. Categorical variables were presented as numbers (percentages) and compared using $\chi^2$ test. Continuous variables were presented as medians (ranges) and compared using Mann-Whitney U test. The McNemar test was used to compare diagnostic performance between PET/CT and CIE, and the accuracy of CIE staging and PET/CT staging. Overall survival (OS) was calculated from the date of the operation or diagnosis until death or last follow-up. Recurrence-free survival (RFS) was calculated from the date of the operation to the date of recurrence or death or last follow-up. Survival analysis was performed using Kaplan-Meier and compared with log-rank test. Multivariate Cox proportional hazards regression analysis was performed to identify independent prognostic factors. Analyses were performed with SPSS software, version 25.0 (IBM Corporation, Armonk, NY, USA). A two-tail P<0.05

**Table 1** Patient characteristics grouped by PET/CT before and after PSM

| Characteristics | All (n=660) | Before PSM, No. (%) | | | After PSM, No. (%) | | |
|---|---|---|---|---|---|---|---|
| | | Group A (n=291) | Group B (n=369) | P value | Group A (n=220) | Group B (n=220) | P value |
| Age (years), median [range]† | 63 [21–89] | 63 [21–88] | 62 [29–89] | 0.609 | 63 [21–88] | 64 [35–89] | 0.415 |
| Gender (male) | 423 (64.1) | 182 (62.5) | 241 (65.3) | 0.462 | 137 (62.3) | 131 (59.5) | 0.558 |
| Clinical symptoms (positive) | 280 (42.4) | 137 (47.1) | 143 (38.8) | 0.032 | 91 (41.4) | 102 (46.4) | 0.291 |
| CA19-9 (≥37 U/mL) | 348 (52.7) | 188 (64.6) | 160 (43.4) | <0.001 | 130 (59.1) | 130 (59.1) | 1.000 |
| CEA (≥5 ng/mL) | 171 (25.9) | 91 (31.3) | 80 (21.7) | 0.005 | 59 (26.8) | 57 (25.9) | 0.829 |
| HBV infection | 218 (33.0) | 73 (25.1) | 145 (39.3) | <0.001 | 59 (26.8) | 54 (24.5) | 0.585 |
| Liver cirrhosis | 116 (17.6) | 35 (12.0) | 81 (22.0) | 0.001 | 30 (13.6) | 30 (13.6) | 1.000 |
| Tumor diameter (≥5 cm) | 387 (58.6) | 196 (67.4) | 191 (51.8) | <0.001 | 135 (61.4) | 142 (64.5) | 0.490 |
| Tumor number (multiple) | 241 (36.5) | 136 (46.7) | 105 (28.5) | <0.001 | 87 (39.5) | 81 (36.8) | 0.556 |
| Vascular invasion | 294 (44.5) | 151 (51.9) | 143 (38.8) | <0.001 | 110 (50.0) | 105 (47.7) | 0.633 |
| Regional LN metastasis | 185 (28.0) | 112 (38.5) | 73 (19.8) | <0.001 | 66 (30.0) | 64 (29.1) | 0.834 |
| Distant metastasis | 125 (18.9) | 74 (25.4) | 51 (13.8) | <0.001 | 43 (19.5) | 43 (19.5) | 1.000 |
| Treatments‡ | | | | | | | |
| Surgical resection | 527 (79.8) | 209 (71.8) | 318 (86.2) | <0.001 | 163 (74.1) | 191 (86.8) | 0.033 |
| TACE + surgical resection | 22 (3.3) | 8 (2.7) | 14 (3.8) | | 8 (3.6) | 6 (2.7) | |
| Liver transplantation | 11 (1.7) | 10 (3.4) | 1 (0.3) | | 9 (4.1) | 1 (0.5) | |
| Radiofrequency ablation | 7 (1.1) | 4 (1.4) | 3 (0.8) | | 4 (1.8) | 1 (0.5) | |
| TACE | 53 (8.0) | 31 (10.7) | 22 (6.0) | | 17 (7.7) | 15 (6.8) | |
| Chemotherapy | 23 (3.5) | 20 (6.9) | 3 (0.8) | | 12 (5.5) | 1 (0.5) | |
| Supportive care | 17 (2.6) | 9 (3.1) | 8 (2.2) | | 7 (3.2) | 5 (2.3) | |

†, compared using Mann-Whitney U test; ‡, treatments are divided into curative treatments (surgical resection, TACE + surgical resection, liver transplantation, and radiofrequency ablation) and non-curative treatments (others) and compared using $\chi^2$ test. PET/CT, positron emission tomography/computed tomography; PSM, propensity score matching; CA19-9, carbohydrate antigen 19-9; CEA, carcinoembryonic antigen; HBV, hepatitis B virus; LN, lymph node; TACE, transcatheter arterial chemoembolization.

was considered statistically significant.

## Results

### *Patient characteristics*

In this study, 660 ICC patients were enrolled (*Figure 1*). The median age was 63 years (range, 21–89 years), with 423 men (64.1%) and 237 women (35.9%). Of these patients, 218 (33.0%) were infected with HBV and 116 (17.6%) had cirrhosis. Two hundred and eighty patients (42.4%) were admitted to hospital for symptoms, including abdominal pain, asthenia, and jaundice. Abnormal serum levels of CA19-9 and CEA were found in 348 patients (52.7%) and 171 patients (25.9%), respectively. The median follow-up time was 22.2 months. Two hundred and ninety-one patients (44.1%) received both PET/CT and CIE (group A), while the rest 369 patients (55.9%) only underwent CIE (group B). Detailed clinicopathological data of patients before and after PSM were listed in *Table 1*.

### *Diagnostic efficiency comparison*

Among 291 patients in group A, regional LN metastases were confirmed in 112 patients pathologically (n=71) or during follow-up imaging (n=41). Sensitivity, specificity

**Table 2** Diagnostic efficiency[†]

| Diagnostic efficiency | Regional LN metastasis | | | Distant metastasis | | |
|---|---|---|---|---|---|---|
| | PET/CT (%) | CIE (%) | P value | PET/CT (%) | CIE (%) | P value |
| Sensitivity | 93/112 (83.0) | 79/112 (70.5) | 0.001 | 65/74 (87.8) | 50/74 (67.6) | <0.001 |
| Specificity | 158/179 (88.3) | 134/179 (74.9) | <0.001 | 207/217 (95.4) | 210/217 (96.8) | 0.508 |
| PPV | 93/114 (81.6) | 79/124 (63.7) | NA | 65/75 (86.7) | 50/57 (87.7) | NA |
| NPV | 158/177 (89.3) | 134/167 (80.2) | NA | 207/216 (95.8) | 210/234 (89.7) | NA |
| Accuracy | 251/291 (86.3) | 213/291 (73.2) | <0.001 | 272/291 (93.5) | 260/291 (89.3) | 0.023 |

[†], compared using McNemar test. LN, lymph node; PET/CT, positron emission tomography/computed tomography; CIE, conventional imaging examination; PPV, positive predictive value; NPV, negative predictive value; NA, not available.

**Table 3** Comparison of diagnostic efficiency with combined criteria

| Diagnostic efficiency | SUVmax only (%) | Criterion I[†] (%) | P value | Criterion II[‡] (%) | P value |
|---|---|---|---|---|---|
| Sensitivity | 93/112 (83.0) | 77/112 (68.8) | <0.001 | 95/112 (84.8) | 0.500 |
| Specificity | 158/179 (88.3) | 166/179 (92.7) | 0.008 | 126/179 (70.4) | <0.001 |
| PPV | 93/114 (81.6) | 77/90 (85.6) | NA | 95/148 (64.2) | NA |
| NPV | 158/177 (89.3) | 166/201 (82.6) | NA | 126/143 (88.1) | NA |
| Accuracy | 251/291 (86.3) | 243/291 (83.5) | 0.152 | 221/291 (75.9) | <0.001 |

[†], SUVmax >2.5 and short-axis diameter ≥1.0 were considered positive; [‡], either SUVmax >2.5 or short-axis diameter ≥1.0 cm was considered positive. SUVmax, maximum standardized uptake value; PPV, positive predictive value; NPV, negative predictive value; NA, not available.

positive predictive value (PPV), negative predictive value (NPV), and accuracy of PET/CT and CIE were 83.0%, 88.3%, 81.6%, 89.3%, 86.3% and 70.5%, 74.9%, 63.7%, 80.2%, 73.2%, respectively. PET/CT was superior to CIE in terms of diagnostic sensitivity (83.0% *vs.* 70.5%, P=0.001), specificity (88.3% *vs.* 74.9%, P<0.001), and accuracy (86.3% *vs.* 73.2%, P<0.001) (*Table 2*).

To achieve better diagnostic efficiency in regional LN metastasis, we attempted to combine SUVmax and short-axis diameter. Both SUVmax >2.5 and short-axis diameter ≥1.0 cm were defined as criterion I, while either SUVmax >2.5 or short-axis diameter ≥1.0 cm was defined as criterion II. Compared with the classical SUVmax cut-off value of 2.5, the criteria I significantly improved specificity (92.7% *vs.* 88.3%, P=0.008), but reduced sensitivity (68.8% *vs.* 83.0%, P<0.001), and the criteria II showed no obvious advantage (*Table 3*). Taken together, these results indicated that SUVmax was a reliable indicator for diagnosing regional LN metastasis.

Totally, distant metastases were confirmed in 74 of the 291 patients pathologically (n=18) or by follow-up imaging (n=56). The most common sites were distant LN metastases (n=48, 64.9%), followed by osseous metastases (n=20, 27.0%), pulmonary metastases (n=16, 21.6%) and peritoneal dissemination (n=12, 16.2%). Sensitivity, specificity, PPV, NPV, and accuracy of PET/CT and CIE were 87.8%, 95.4%, 86.7%, 95.8%, 93.5% and 67.6%, 96.8%, 87.7%, 89.7%, 89.3%, respectively. Indeed, PET/CT showed significantly higher sensitivity (87.8% *vs.* 67.6%, P<0.001) and accuracy (93.5% *vs.* 89.3%, P=0.023) than CIE, with comparable specificity (95.4% *vs.* 96.8%, P=0.508) (*Table 2*).

### *Preoperative staging and treatment allocation*

After incorporating PET/CT in group A, the accuracy of preoperative staging was significantly improved from 60.1% to 71.8% (P<0.001). The treatment strategies of 17 cases (5.8%) were modified including avoiding unnecessary surgery in 13 cases (*Figure 2*), performing extended LN dissection in 3 cases, and treating osseous metastasis using γ knife in

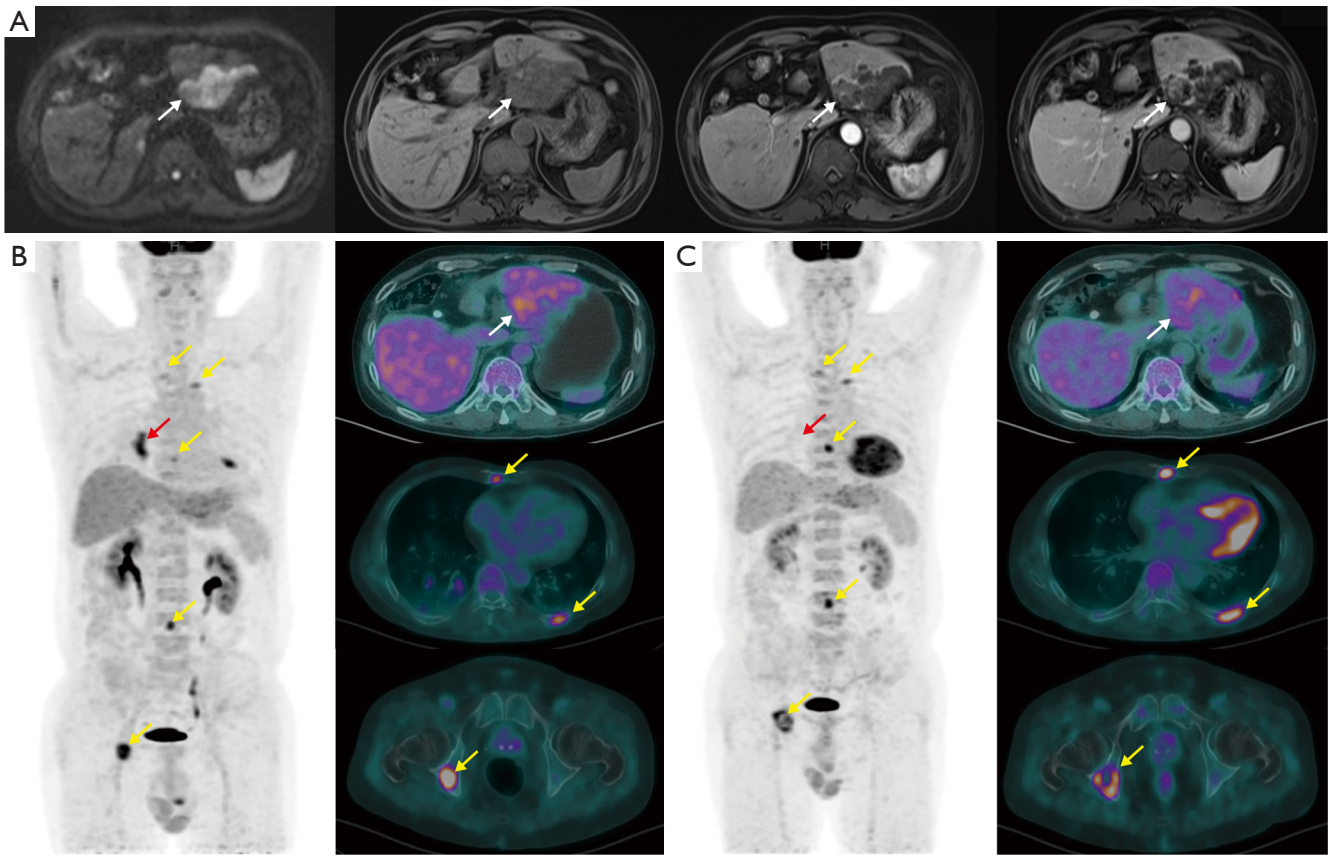


**Figure 2** An example of treatment modification by PET/CT. A 60-year-old patient was admitted to our hospital for abdominal discomfort. (A) Abdominal contrast-enhanced MRI detected a cystic-solid mass (7.6 cm × 4.8 cm, white arrows) in the left lateral lobe. The initial treatment was surgical resection. (B) PET/CT images showed the primary lesion and multiple osseous metastases (right ilium, rib, sternum, thoracic vertebra, and lumbar vertebra, yellow arrows). The tumor staging was upgraded from TNM IIIB to TNM IV, thus the patient received chemotherapy instead of resection. (C) After 2 months, PET/CT reexamination showed that the pulmonary inflammatory absorbed (red arrow), and the volume and metabolism of partial osseous metastases deteriorated (rib, sternum, right ilium). PET/CT, positron emission tomography/computed tomography; MRI, magnetic resonance imaging; TNM, tumor-node-metastasis.

1 case. The details were listed in Table S3.

Totally, PET/CT identified new lesions in 62 cases, consisting of regional LN metastases, distant metastases, and both metastases in 17, 39, and 6 cases, respectively. The new lesions in 50 cases (80.6%) were proved to be "true". Meanwhile, PET/CT modified preoperative staging in 68 cases (upgrade in 36 cases and downgrade in 32 cases), 75.0% of which were proved correct. Although PET/CT showed higher diagnostic performance than CIE on the N- and M-staging, there were still some false positives and false negatives which resulted in stage migrations.

Notably, PET/CT played unique roles among different TNM stages (*Table 4*). In stages IA, IB, and II patients, PET/CT detected new lesions in 1/43 (2.3%), 2/20 (10.0%), and 20/78 (25.6%) of cases, respectively, indicating that PET/CT played an increasingly important role with the increase of tumor burden. For TNM stage III patients, PET/CT could not only detect new lesions in 13/93 (14.0%) of cases but also reevaluate enlarged LNs in 29/93 (31.2%) of cases. More new distant lesions in 26/57 (45.6%) of cases were detected and tumor burden was estimated correctly by PET/CT in TNM stage IV patients.

### *Prognosis prediction*

In survival analyses, 13 patients who died after operations within three months were excluded. For the remaining 278 patients in group A, 210 patients received surgery

**Table 4** Influences of PET/CT according to baseline CIE staging

| Influences of PET/CT | CIE staging, No. (%) | | | | | Total (n=291), No. (%) |
|---|---|---|---|---|---|---|
| | IA (n=43) | IB (n=20) | II (n=78) | III (n=93) | IV (n=57) | |
| New lesions | | | | | | |
| Regional LN metastasis | 1 (2.3) | 2 (10.0) | 13 (16.7) | 0 | 1 (1.8) | 17 (5.8) |
| Distant metastasis | 0 | 0 | 3 (3.8) | 13 (14.0) | 23 (40.4) | 39 (13.4) |
| Both metastases[†] | 0 | 0 | 4 (5.1) | 0 | 2 (3.5) | 6 (2.1) |
| Staging modification | | | | | | |
| Upgrade | 1 (2.3) | 2 (10.0) | 20 (25.6) | 13 (14.0) | 0 | 36 (12.4) |
| Downgrade | 0 | 0 | 0 | 29 (31.2) | 3 (5.3) | 32 (11.0) |
| Treatment modification | | | | | | |
| Avoiding unnecessary surgery | 0 | 0 | 2 (2.6) | 6 (6.5) | 5 (8.8) | 13 (4.5) |
| Performing extended lymph node dissection | 0 | 0 | 1 (1.3) | 2 (2.2) | 0 | 3 (1.0) |
| Treating osseous metastasis using γ knife | 0 | 0 | 0 | 0 | 1 (1.8) | 1 (0.3) |

[†], both metastases include regional LN metastasis and distant metastasis. PET/CT, positron emission tomography/computed tomography; CIE, conventional imaging examination; LN, lymph node.

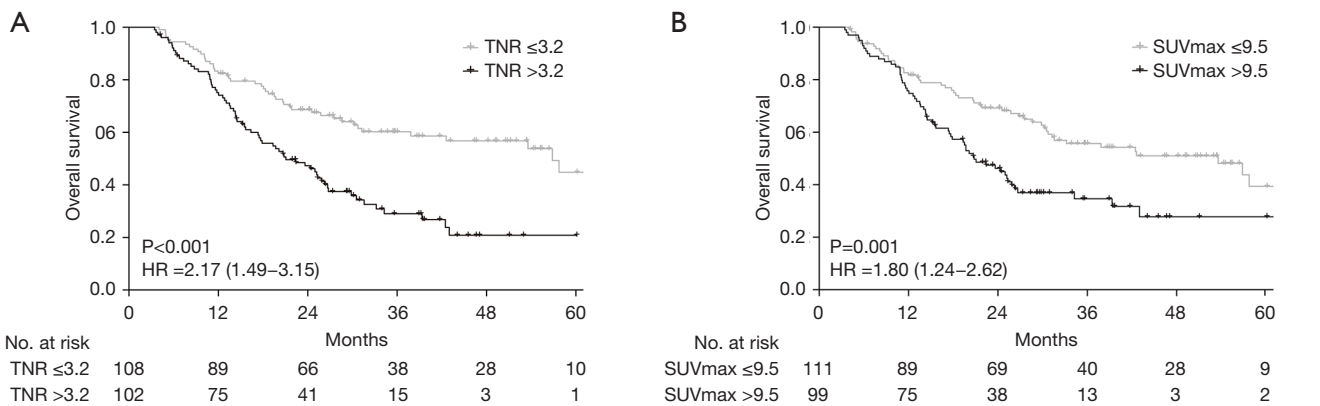


**Figure 3** Kaplan-Meier curves for OS by TNR and tumor SUVmax. Kaplan-Meier curves based on TNR (A) and tumor SUVmax (B) for OS in patients receiving surgery (n=210). P values were calculated from the log-rank test. HR, hazard ratio; TNR, tumor-to-non-tumor ratio; SUVmax, maximum standardized uptake value; OS, overall survival.

and the optimal tumor SUVmax and TNR cut-off values were 9.5 and 3.2, as determined by minimum P values of OS. Patients with high TNR had significantly shorter OS [hazard ratio (HR) =2.17; 95% confidence interval (CI): 1.49–3.15; P<0.001] (*Figure 3A*) and RFS (HR =1.93; 95% CI: 1.40–2.67; P<0.001) (Figure S1A) than those with low TNR. Similarly, patients with high tumor SUVmax had significantly shorter OS (HR =1.80; 95% CI: 1.24–2.62; P=0.001) (*Figure 3B*) and RFS (HR =1.69; 95% CI: 1.23–2.34; P<0.001) (Figure S1B). Intriguingly, TNR, instead of tumor SUVmax, remained significant on multivariate analyses for both OS (HR =1.60; 95% CI: 1.07–2.38; P=0.023) and RFS (HR =1.63; 95% CI: 1.18–2.25; P=0.003) after adjusting for clinicopathologic variables, suggesting that TNR might be a better prognostic indicator than tumor SUVmax (Tables S4,S5). For all patients with various treatments, high TNR and tumor SUVmax still predicted poor outcomes, indicating

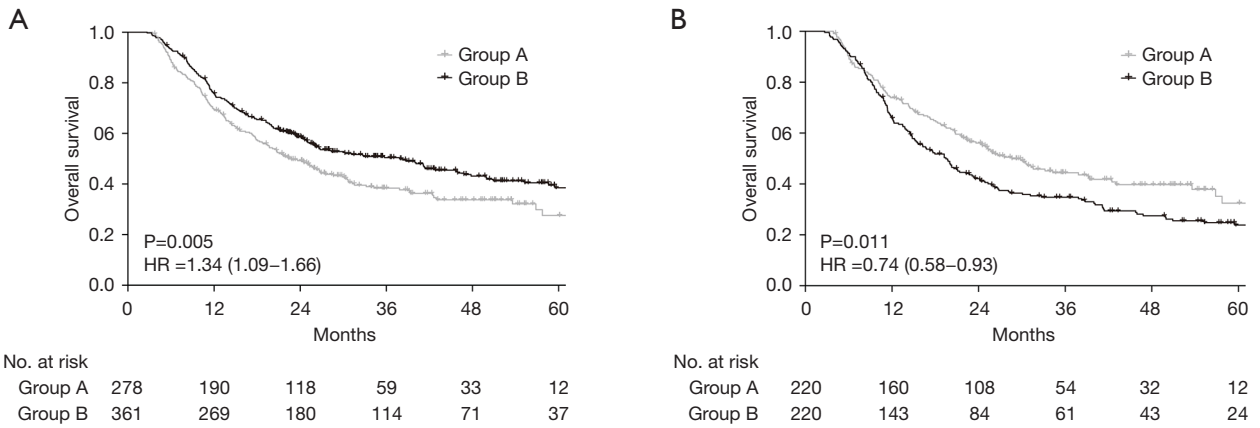


**Figure 4** OS comparison before and after PSM. Kaplan-Meier curves for OS in group A and group B before PSM (A) and after PSM (B). P values were calculated from the log-rank test. HR, hazard ratio; OS, overall survival; PSM, propensity score matching.

the robustness of two indicators (Figure S1C,S1D).

CA19-9 has been widely used for predicting outcomes in ICC (24), and thus we divided patients into four subgroups according to the CA19-9 and TNR status. Patients with abnormal CA19-9 and high TNR had the worst OS, while patients with normal CA19-9 and low TNR had the best OS (Figure S1E). Notably, high TNR still predicted poor OS irrespective of patients with normal CA19-9 (HR =2.57; 95% CI: 1.21–5.44; P=0.004) or abnormal CA19-9 (HR =1.78; 95% CI: 1.16–2.75; P=0.009), indicating the complementarity of CA19-9 and TNR.

### *Survival benefit*

To explore the survival benefit of performing PET/CT, we compared the OS of patients performing PET/CT (group A) and those without PET/CT (group B). However, the clinicopathological features of patients in group A were more aggressive than group B (*Table 1*). As excepted, patients in group A had significantly shorter OS than group B (HR =1.34; 95% CI: 1.09–1.66; P=0.005) (*Figure 4A*). When performing multivariate analysis, we found undergoing PET/CT was an independent protective factor for OS (HR =0.78; 95% CI: 0.62–0.97; P=0.028) (Table S6). Thus, we exploratively applied PSM to reduce select biases and confounding factors. There remained 220 patients in both groups A and B with similar clinicopathological characteristics (*Table 1*). The treatment allocation was significantly different where curative treatments were performed in 83.6% of patients in group A and 90.5% in group B (P=0.033), authenticating the impact of PET/CT on clinical treatment strategy. Indeed, patients in group A had significantly longer OS than group B (HR =0.74; 95% CI: 0.58–0.93; P=0.011) (*Figure 4B*) after PSM, possibly due to the precise evaluation of tumor burden and subsequent proper treatment selection.

## Discussion

In this retrospective analysis of a large cohort of ICC patients, PET/CT was proved to be superior to conventional imaging in diagnosing regional LN metastasis and distant metastasis. After performing PET/CT, new lesions were detected and tumor staging was refined, leading to optimization of treatment allocation and improvement in patient clinical outcomes. Meanwhile, high tumor SUVmax or TNR indicated increased recurrence and dismal survival. As such, PET/CT should be recommended for clinical practice, considering the extremely high metastatic rate of ICC.

LN metastasis is the most common metastatic route of ICC and signifies a dismal outcome (25). Nonetheless, the benefit of routine lymphadenectomy, especially in those with negative clinical diagnosis, is still controversial due to the postoperative morbidity and uncertainty of survival benefit (26-29). Accurate imaging assessment of LN metastasis is an urgent need for ICC patients, but the comparison of diagnostic performance of PET/CT and CIE remains controversial (11,13,19). Using the largest ICC cohort to date, we confirmed the diagnostic superiority of PET/CT to CIE in LN metastasis. As such, the comparison between routine lymphadenectomy and selective lymphadenectomy under the guidance of PET/CT

is worthy of further prospective clinical trials.

Preoperative staging is decisive to the treatment strategies of cancer patients. A prospective, multi-center trial in lymphoma has demonstrated that PET/CT facilitated correct tumor staging and subsequent clinical management, leading to lower mortality (30). Herein, PET/CT significantly enhanced the accuracy of preoperative staging of ICC from 60.1% to 71.8% by more accurate assessment of metastasis. In addition to treatment modification in 5.8% of ICC patients, precise evaluation of tumor burden by PET/CT may also bring clinical benefits including the scheme optimization of systemic therapy and surveillance of therapeutic effects. Meanwhile, we showed unique roles of PET/CT in different TNM stages due to either detecting new lesions or reevaluating enlarged LNs on CIE. PET/CT has relatively limited effect on early-stage patients that 2.3% of stage IA patients and 10.0% of stage IB patients were upgraded. However, the numbers of stages IA and IB patients were relatively small in our cohort (n=43 and 20, respectively). Thus, the application of PET/CT in early-stage patients remains to be further explored. In stages II and III patients, PET/CT played an important role in preoperative staging modification. For stage IV patients, PET/CT detected more new distant lesions in nearly half of cases which was essential for estimating tumor burden and monitoring tumor progression. As PET/CT played an increasingly important role in advanced ICC, we proposed that the greater the tumor burden, the more necessary the PET/CT examination.

The prognostic role of tumor SUVmax has been reported in biliary cancers (11). Here, we compared the prognostic values of TNR with SUVmax, and found TNR was a better prognosticator in ICC. Notably, TNR could stratify patients with either normal or abnormal CA19-9 into high or low risk subgroups, suggesting the potential of the combined application of CA19-9 and TNR to predict clinical outcomes of ICC patients.

Beyond tumor staging, PET/CT has been widely used in detecting recurrence and monitoring treatment effects (31). In this regard, utilizing $^{18}$F-FDG PET with deep learning model could predict the sensitivity of immunotherapy in lung adenocarcinoma (32). As molecular targeted therapy and immunotherapy have becoming increasingly important in ICC (33-36), such scenario may come to a reality in the near future. Apart from $^{18}$F-FDG, more novel imaging agents such as $^{11}$C-fluorocholine, $^{18}$F-fluoroestradiol, and $^{18}$F-fluorothymidine, have been tested and applied in cancers (37,38). Targeting tumor-specific biomarkers and metabolism with optimal imaging agent are promising in PET/CT, such as the $^{68}$Ga-prostate specific membrane antigen (PSMA) PET in detecting metastasis of prostate cancer (39). Altogether, PET/CT has great potential in clinical management of cancer patients including ICC.

Although this study was a single-center, retrospective analysis, we chose a consecutive patient cohort and applied PSM to reduce the potential bias. Some extrahepatic lesions in patients without surgical resection or biopsy were not available for pathological diagnosis. To resolve this issue, we used RECIST to confirm metastasis by follow-up imaging. Even the resected LNs are difficult to precisely match the corresponding LNs in preoperative images retrospectively, thus we evaluated the diagnostic efficiency of PET/CT and CIE at patient level rather than at lesion level, which may enhance their diagnostic sensitivity but reduce specificity.

In conclusion, this study demonstrated the diagnostic value of PET/CT over conventional imaging on the N- and M-staging in ICC patients. PET/CT played significant roles in different TNM stages by detecting new lesions, reevaluating equivocal lesions, modifying tumor staging, and optimizing treatment strategy. Further data are needed to support the survival benefit of PET/CT in ICC patients.

## Acknowledgments

*Funding:* The study was supported by project grants from the National Natural Science Foundation of China (Nos. 91859105, and 81961128025), the Program of Shanghai Academic Research Leader (No. 19XD1420700), the Science and Technology Commission of Shanghai Municipality (No. 20JC1418900), and the Shanghai Municipal Key Clinical Specialty.

## Footnote

*Reporting Checklist:* The authors have completed the STARD reporting checklist. Available at https://hbsn.amegroups.com/article/view/10.21037/hbsn-21-25/rc

*Data Sharing Statement:* Available at https://hbsn.amegroups.com/article/view/10.21037/hbsn-21-25/dss

*Conflicts of Interest:* All authors have completed the ICMJE uniform disclosure form (available at https://hbsn.amegroups.com/article/view/10.21037/hbsn-21-25/coif). The authors report that the study was supported by project grants from the National Natural Science Foundation of

China (Nos. 91859105, and 81961128025), the Program of Shanghai Academic Research Leader (No. 19XD1420700), the Science and Technology Commission of Shanghai Municipality (No. 20JC1418900), and the Shanghai Municipal Key Clinical Specialty. The authors have no other conflicts of interest to declare.

*Ethical Statement*: The authors are accountable for all aspects of the work in ensuring that questions related to the accuracy or integrity of any part of the work are appropriately investigated and resolved. The study was conducted in accordance with the Declaration of Helsinki (as revised in 2013). The study was approved by institutional ethics board of Zhongshan Hospital, Fudan University (No. B2020-322) and informed consent was taken from all individual participants.



## References

1. Bray F, Ferlay J, Soerjomataram I, et al. Global cancer statistics 2018: GLOBOCAN estimates of incidence and mortality worldwide for 36 cancers in 185 countries. CA Cancer J Clin 2018;68:394-424.
2. Njei B. Changing pattern of epidemiology in intrahepatic cholangiocarcinoma. Hepatology 2014;60:1107-8.
3. Spolverato G, Bagante F, Weiss M, et al. Comparative performances of the 7th and the 8th editions of the American Joint Committee on Cancer staging systems for intrahepatic cholangiocarcinoma. J Surg Oncol 2017;115:696-703.
4. Graafland NM, Leijte JA, Valdés Olmos RA, et al. Scanning with 18F-FDG-PET/CT for detection of pelvic nodal involvement in inguinal node-positive penile carcinoma. Eur Urol 2009;56:339-45.
5. Angelini A, Ceci F, Castellucci P, et al. The role of 18F-FDG PET/CT in the detection of osteosarcoma recurrence. Eur J Nucl Med Mol Imaging 2017;44:1712-20.
6. Grootjans W, de Geus-Oei LF, Troost EG, et al. PET in the management of locally advanced and metastatic NSCLC. Nat Rev Clin Oncol 2015;12:395-407.
7. Benson AB, D'Angelica MI, Abbott DE, et al. Guidelines Insights: Hepatobiliary Cancers, Version 2.2019. J Natl Compr Canc Netw 2019;17:302-10.
8. Valle JW, Borbath I, Khan SA, et al. Biliary cancer: ESMO Clinical Practice Guidelines for diagnosis, treatment and follow-up. Ann Oncol 2016;27:v28-37.
9. Weber SM, Ribero D, O'Reilly EM, et al. Intrahepatic cholangiocarcinoma: expert consensus statement. HPB (Oxford) 2015;17:669-80.
10. Bridgewater J, Galle PR, Khan SA, et al. Guidelines for the diagnosis and management of intrahepatic cholangiocarcinoma. J Hepatol 2014;60:1268-89.
11. Lamarca A, Barriuso J, Chander A, et al. 18F-fluorodeoxyglucose positron emission tomography (18FDG-PET) for patients with biliary tract cancer: Systematic review and meta-analysis. J Hepatol 2019;71:115-29.
12. Jiang L, Tan H, Panje CM, et al. Role of 18F-FDG PET/CT Imaging in Intrahepatic Cholangiocarcinoma. Clin Nucl Med 2016;41:1-7.
13. Lee SW, Kim HJ, Park JH, et al. Clinical usefulness of 18F-FDG PET-CT for patients with gallbladder cancer and cholangiocarcinoma. J Gastroenterol 2010;45:560-6.
14. Petrowsky H, Wildbrett P, Husarik DB, et al. Impact of integrated positron emission tomography and computed tomography on staging and management of gallbladder cancer and cholangiocarcinoma. J Hepatol 2006;45:43-50.
15. Ma KW, Cheung TT, She WH, et al. Diagnostic and Prognostic Role of 18-FDG PET/CT in the Management of Resectable Biliary Tract Cancer. World J Surg 2018;42:823-34.
16. Cho KM, Oh DY, Kim TY, et al. Metabolic Characteristics of Advanced Biliary Tract Cancer Using 18F-Fluorodeoxyglucose Positron Emission Tomography and Their Clinical Implications. Oncologist 2015;20:926-33.
17. Furukawa H, Ikuma H, Asakura K, et al. Prognostic importance of standardized uptake value on F-18 fluorodeoxyglucose-positron emission tomography in biliary tract carcinoma. J Surg Oncol 2009;100:494-9.
18. Corvera CU, Blumgart LH, Akhurst T, et al. 18F-fluorodeoxyglucose positron emission tomography influences management decisions in patients with biliary cancer. J Am Coll Surg 2008;206:57-65.
19. Kim JY, Kim MH, Lee TY, et al. Clinical role of 18F-FDG PET-CT in suspected and potentially operable

 

cholangiocarcinoma: a prospective study compared with conventional imaging. Am J Gastroenterol 2008;103:1145-51.
20. Park TG, Yu YD, Park BJ, et al. Implication of lymph node metastasis detected on 18F-FDG PET/CT for surgical planning in patients with peripheral intrahepatic cholangiocarcinoma. Clin Nucl Med 2014;39:1-7.
21. Jeong IG, Hong S, You D, et al. FDG PET-CT for lymph node staging of bladder cancer: a prospective study of patients with extended pelvic lymphadenectomy. Ann Surg Oncol 2015;22:3150-6.
22. Eisenhauer EA, Therasse P, Bogaerts J, et al. New response evaluation criteria in solid tumours: revised RECIST guideline (version 1.1). Eur J Cancer 2009;45:228-47.
23. Chun YS, Pawlik TM, Vauthey JN. 8th Edition of the AJCC Cancer Staging Manual: Pancreas and Hepatobiliary Cancers. Ann Surg Oncol 2018;25:845-7.
24. Wang Y, Li J, Xia Y, et al. Prognostic nomogram for intrahepatic cholangiocarcinoma after partial hepatectomy. J Clin Oncol 2013;31:1188-95.
25. Ji GW, Zhang YD, Zhang H, et al. Biliary Tract Cancer at CT: A Radiomics-based Model to Predict Lymph Node Metastasis and Survival Outcomes. Radiology 2019;290:90-8.
26. Sahara K, Tsilimigras DI, Merath K, et al. Therapeutic Index Associated with Lymphadenectomy Among Patients with Intrahepatic Cholangiocarcinoma: Which Patients Benefit the Most from Nodal Evaluation? Ann Surg Oncol 2019;26:2959-68.
27. Zhou R, Lu D, Li W, et al. Is lymph node dissection necessary for resectable intrahepatic cholangiocarcinoma? A systematic review and meta-analysis. HPB (Oxford) 2019;21:784-92.
28. Mao K, Liu J, Sun J, et al. Patterns and prognostic value of lymph node dissection for resected perihilar cholangiocarcinoma. J Gastroenterol Hepatol 2016;31:417-26.
29. Morine Y, Shimada M. The value of systematic lymph node dissection for intrahepatic cholangiocarcinoma from the viewpoint of liver lymphatics. J Gastroenterol 2015;50:913-27.
30. Metser U, Prica A, Hodgson DC, et al. Effect of PET/CT on the Management and Outcomes of Participants with Hodgkin and Aggressive Non-Hodgkin Lymphoma: A Multicenter Registry. Radiology 2019;290:488-95.
31. Jo J, Kwon HW, Park S, et al. Prospective Evaluation of the Clinical Implications of the Tumor Metabolism and Chemotherapy-Related Changes in Advanced Biliary Tract Cancer. J Nucl Med 2017;58:1255-61.
32. Park C, Na KJ, Choi H, et al. Tumor immune profiles noninvasively estimated by FDG PET with deep learning correlate with immunotherapy response in lung adenocarcinoma. Theranostics 2020;10:10838-48.
33. Abou-Alfa GK, Sahai V, Hollebecque A, et al. Pemigatinib for previously treated, locally advanced or metastatic cholangiocarcinoma: a multicentre, open-label, phase 2 study. Lancet Oncol 2020;21:671-84.
34. Abou-Alfa GK, Macarulla T, Javle MM, et al. Ivosidenib in IDH1-mutant, chemotherapy-refractory cholangiocarcinoma (ClarIDHy): a multicentre, randomised, double-blind, placebo-controlled, phase 3 study. Lancet Oncol 2020;21:796-807.
35. Klein O, Kee D, Nagrial A, et al. Evaluation of Combination Nivolumab and Ipilimumab Immunotherapy in Patients With Advanced Biliary Tract Cancers: Subgroup Analysis of a Phase 2 Nonrandomized Clinical Trial. JAMA Oncol 2020;6:1405-9.
36. Zhou J, Fan J, Shi G, et al. 56P Anti-PD1 antibody toripalimab, lenvatinib and gemox chemotherapy as first-line treatment of advanced and unresectable intrahepatic cholangiocarcinoma: A phase II clinical trial. Ann Oncol 2020;31:S262-3.
37. Farwell MD, Pryma DA, Mankoff DA. PET/CT imaging in cancer: current applications and future directions. Cancer 2014;120:3433-45.
38. Katzenellenbogen JA. PET Imaging Agents (FES, FFNP, and FDHT) for Estrogen, Androgen, and Progesterone Receptors to Improve Management of Breast and Prostate Cancers by Functional Imaging. Cancers (Basel) 2020;12:2020.
39. Perera M, Papa N, Roberts M, et al. Gallium-68 Prostate-specific Membrane Antigen Positron Emission Tomography in Advanced Prostate Cancer-Updated Diagnostic Utility, Sensitivity, Specificity, and Distribution of Prostate-specific Membrane Antigen-avid Lesions: A Systematic Review and Meta-analysis. Eur Urol 2020;77:403-17.

**Cite this article as:** Lin Y, Chong H, Song G, Zhang C, Dong L, Aye L, Liang F, Yang S, Zeng M, Ding G, Zhang S, Shi J, Ke A, Wang X, Zhou J, Fan J, Gao Q. The influence of $^{18}$F-fluorodeoxyglucose positron emission tomography/computed tomography on the N- and M-staging and subsequent clinical management of intrahepatic cholangiocarcinoma. HepatoBiliary Surg Nutr 2022;11(5):684-695. doi: 10.21037/hbsn-21-25

## Supplementary

**Table S1** Imaging examinations

| Imaging examinations | Group A (n=291) | Group B (n=369) | Total (n=660) |
|---|---|---|---|
| PET/CT | 291 (100.0) | 0 | 291 (44.1) |
| Abdominal contrast-enhanced MRI | 271 (93.1) | 344 (93.2) | 615 (93.2) |
| Abdominal contrast-enhanced CT | 77 (26.5) | 56 (15.2) | 133 (20.2) |
| Chest CT | 63 (21.6) | 105 (28.5) | 168 (25.5) |
| Chest radiography | 228 (78.4) | 264 (71.5) | 492 (74.5) |

PET/CT, positron emission tomography/computed tomography; MRI, magnetic resonance imaging; CT, computed tomography.


https://dx.doi.org/10.21037/hbsn-21-25

**Table S2** Sequences and parameters of abdominal contrast-enhanced MRI[†]

| MR machines | Parameters | TR (ms) | TE (ms) | BW (Hz/pixel) | FOV (mm × mm) | Acquisition matrix | Slice thickness (mm) | Flip angle (°) |
|---|---|---|---|---|---|---|---|---|
| UIHMR 770, United Imaging, China; 3.0 Tesla | T2WI-FS | 2,000 | 106.2 | 365 | 380×380 | 256×256 | 6.0 | 100 |
| | DWI (b=0, 500 $mm^2/s$) | 5,000 | 66.3 | 2,370 | 380×300 | 128 ×128 | 6.0 | 90 |
| | T1WI IP/OP | 4.2 | 1.2/2.5 | 900 | 400×300 | 288×224 | 3.0 | 10 |
| | T1WI-FS tra | 3.3 | 1.5 | 650 | 400×270 | 320 ×288 | 3.0 | 10 |
| | T1WI-FS cor | 3.3 | 1.5 | 600 | 340×340 | 270×270 | 3.0 | 10 |
| Magnetom Verio, Siemens Healthcare, Germany; 3.0 Tesla | T2WI-FS | 2,500 | 83 | 260 | 380×330 | 320×165 | 5.5 | 122 |
| | DWI (b=0, 500 $mm^2/s$) | 3,400 | 70 | 2,442 | 380×285 | 128×80 | 6.0 | 90 |
| | T1WI IP/OP | 207 | 2.3/3.7 | 930 | 380×285 | 256×141 | 5.5 | 70 |
| | T1WI-FS tra | 4.2 | 1.4 | 390 | 380×285 | 352×200 | 3.0 | 9 |
| | T1WI-FS cor | 4.1 | 1.5 | 9 | 380×380 | 384×269 | 3.0 | 9 |
| Magnetom Avanto, Siemens Healthcare, Germany; 1.5 Tesla | T2WI-FS | 3,100 | 84 | 260 | 360×304 | 256×173 | 7.0 | 150 |
| | DWI (b=0, 500 $mm^2/s$) | 2,800 | 66 | 1,502 | 360×315 | 112×128 | 7.0 | 90 |
| | T1WI IP/OP | 118 | 2.0/5.0 | 376/416 | 360×270 | 256×134 | 7.0 | 70 |
| | T1WI-FS tra | 5.1 | 2.4 | 299 | 380×264 | 288×130 | 4.0 | 10 |
| | T1WI-FS cor | 5.2 | 2.4 | 300 | 380×308 | 128×112 | 5.0 | 10 |
| Magnetom Aera, Siemens Healthcare, Germany; 1.5 Tesla | T2WI-FS | 4,918 | 106 | 195 | 380×380 | 384×273 | 5.5 | 160 |
| | DWI (b=0, 500 $mm^2/s$) | 5,100 | 55 | 1735 | 380×297 | 192×120 | 5.5 | 90 |
| | T1WI IP/OP | 6.9 | 2.4/4.8 | 435/480 | 380×297 | 320×188 | 4.0 | 10 |
| | T1WI-FS tra | 3.5 | 1.4 | 405 | 380×281 | 352×195 | 3.0 | 10 |
| | T1WI-FS cor | 4.4 | 2.0 | 410 | 380×350 | 320×320 | 3.0 | 10 |
| UIHMR 560, United Imaging, China; 1.5 Tesla | T2WI-FS | 2,693 | 85.6 | 260 | 380×360 | 288×201 | 6.0 | 150 |
| | DWI (b=0, 500 $mm^2/s$) | 280.7 | 75.7 | 1,720 | 380×300 | 128×115 | 6.0 | 90 |
| | T1WI IP/OP | 115.8 | 2.2/4.4 | 360 | 380×290 | 288×230 | 6.0 | 70 |
| | T1WI-FS tra | 4.5 | 2.2 | 400 | 400×280 | 256×192 | 3.5 | 10 |
| | T1WI-FS cor | 4.5 | 2.2 | 360 | 450×350 | 256×125 | 3.0 | 10 |

[†], the sequences include axial respiratory-triggered T2WI-FS, breath-hold gradient echo T1WI IP/OP, breath-hold DWI with b values of 0 and 500 $mm^2/s$, T1-weighted 3D-volumetric interpolated breath-hold examination imaging with transverse and coronal fat suppressed (T1WI-FS tra, T1WI-FS cor), dynamic contrast-enhanced imaging (pre-contrast, arterial, portal venous and delayed phases). MRI, magnetic resonance imaging; TR, repetition time; TE, echo time; BW, bandwidth; FOV, field of view; T2WI-FS, T2-weighted imaging fat suppressed fast spin echo sequence; T1WI IP/OP, T1-weighted in-phase and opposed-phase imaging; DWI, diffusion-weighted imaging.


https://dx.doi.org/10.21037/hbsn-21-25

**Table S3** Impact of PET/CT on treatment allocation

| Patient | Findings on CIE | Findings on PET/CT | Impact on treatment allocation | Follow-up (up until May 2020) |
|---|---|---|---|---|
| 1 | Multiple tumors in the liver and enlarged hilar lymph nodes | Right $7^{th}$, $9^{th}$ posterior costal and right acetabular metastasis | Avoiding unnecessary surgery | Osseous metastases progressed and the patient died in 10.5 months |
| 2 | Multiple tumors in the left lobe of liver and enlarged hilar and para-aortic lymph nodes | Increased FDG uptake in para-aortic and pelvic lymph nodes and suspicious pulmonary metastasis | Avoiding unnecessary surgery | The pulmonary nodule remained stable but lymph node metastases progressed and the patient died in 6.3 months |
| 3 | Multiple tumors in the liver and enlarged hilar lymph nodes | $5^{th}$ thoracic vertebra metastasis | Avoiding unnecessary surgery | Osseous metastases progressed and the patient died in 10.5 months |
| 4 | Multiple tumors in the right lobe of liver and enlarged hilar and lymph nodes | Increased FDG uptake in para-aortic lymph nodes and suspicious pulmonary metastasis | Avoiding unnecessary surgery | Metastatic lesions progressed and the patient died in 21.6 months |
| 5 | Multiple tumors in the liver and small pulmonary nodules in chest radiography | Pulmonary metastases | Avoiding unnecessary surgery | pulmonary nodules progressed and the patient died in 17.2 months |
| 6 | A tumor in the left external lobe of liver and enlarged hilar lymph nodes | Multiple osseous metastases | Avoiding unnecessary surgery | Osseous metastases progressed and the patient died in 17.8 months |
| 7 | A tumor in the left external lobe of liver and suspicious right $5^{th}$ rib metastasis | Multiple osseous metastases | Avoiding unnecessary surgery | Osseous metastases progressed and the patient died in 9.9 months |
| 8 | A tumor in the right posterior lobe of liver and enlarged hilar and para-aortic lymph nodes | Increased FDG uptake in para-aortic and left clavicular lymph nodes | Avoiding unnecessary surgery | The left clavicular lymph node metastasis was confirmed by biopsy and the patient died in 6 months |
| 9 | Multiple tumors in the liver and enlarged para-aortic lymph nodes | Increased FDG uptake in para-aortic, pelvic, and left clavicular lymph node; pelvic implantation metastasis; right ischial metastasis | Avoiding unnecessary surgery | Metastatic lesions progressed and the patient died in 4.6 months |
| 10 | Multiple tumors in the left lobe of liver | Multiple osseous metastases | Avoiding unnecessary surgery | Osseous metastases progressed and the patient died in 9.1 months |
| 11 | Multiple tumors in the right lobe of liver | Right retroperitoneal implantation metastasis | Avoiding unnecessary surgery | Metastatic lesions progressed and the patient died in 14.9 months |
| 12 | A tumor in the left external lobe of liver | suspicious pulmonary metastasis | Avoiding unnecessary surgery | The pulmonary nodule progressed and the patient died in 6.8 months |
| 13 | Multiple tumors in the liver and enlarged hilar lymph nodes | Increased FDG uptake in para-aortic lymph nodes; peritoneal and pelvic implantation metastases; multiple osseous metastases | Avoiding unnecessary surgery | Metastatic lesions progressed and the patient died in 5.6 months |
| 14 | A tumor in the right lobe of liver and enlarged hilar lymph nodes | Increased FDG uptake in pelvic lymph nodes and peritoneal metastases | Expanding the scope of lymphadenectomy | The surgically resected peritoneal nodules and pelvic lymph nodes were confirmed metastasis pathologically and the patient relapsed in 5.1 months and died in 18.7 months |
| 15 | A tumor in the right lobe of liver | Increased FDG uptake in hilar and left cardia lymph nodes | Expanding the scope of lymphadenectomy | The surgically resected lymph nodes were confirmed metastasis pathologically and the patient relapsed in 25.3 months and was still alive in 35.6 months |
| 16 | A tumor in the left external lobe of liver and enlarged hilar lymph nodes | Increased FDG uptake in para-aortic lymph nodes | Expanding the scope of lymphadenectomy | The resected para-aortic lymph node was confirmed metastasis pathologically, but pericardial invasion was found during the operation, and the patient died in 3.4 months |
| 17 | A tumor in the right lobe of liver | Left ilium metastasis | Treating osseous metastasis using γ knife | Multiple osseous metastases were found by PET/CT in 23.6 months and the patient was still alive in 27.6 months |

PET/CT, positron emission tomography/computed tomography; CIE, conventional imaging examination; FDG, fluorodeoxyglucose.



https://dx.doi.org/10.21037/hbsn-21-25

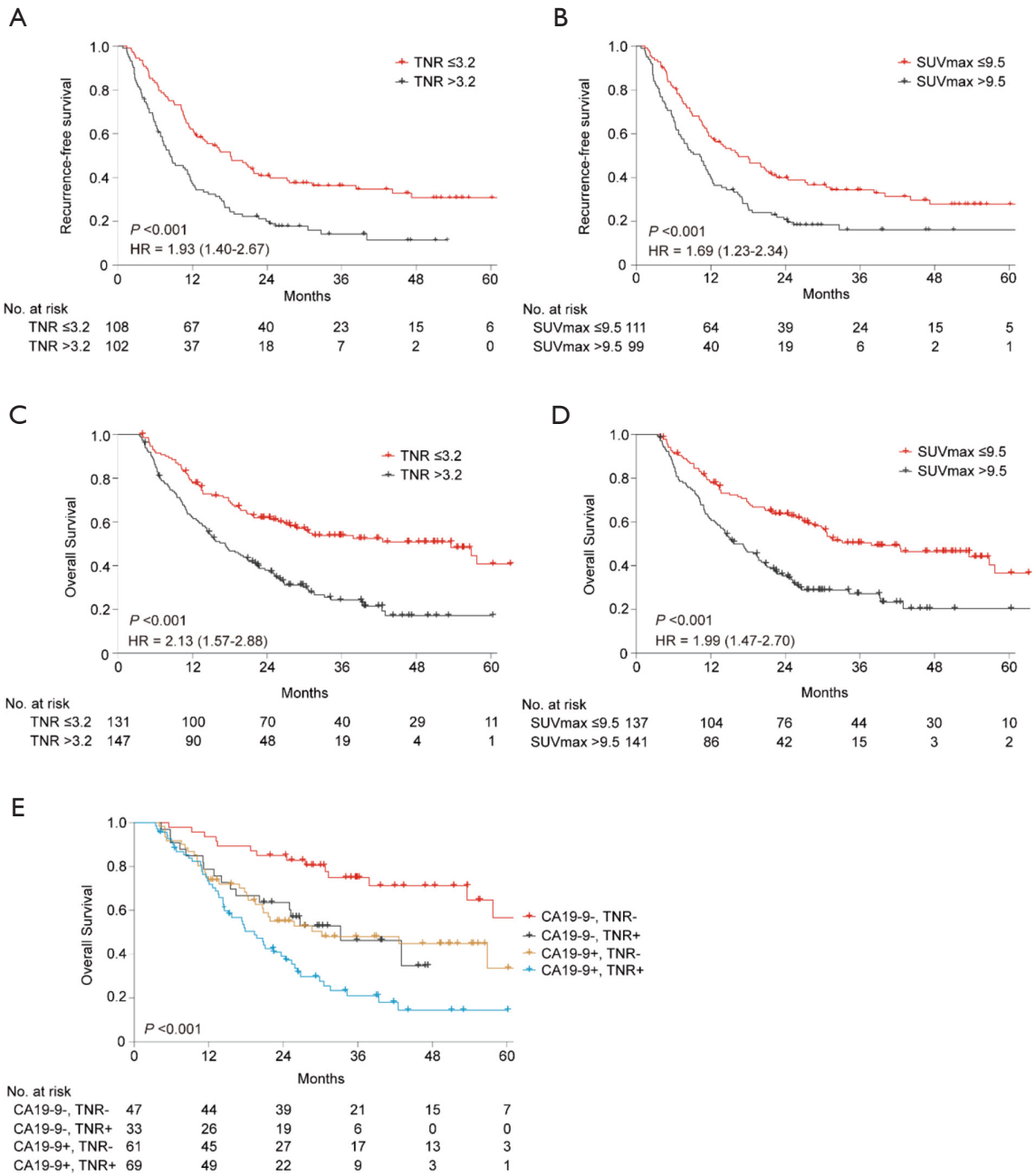


**Figure S1** Prognostic stratification by TNR, tumor SUVmax, and CA19-9. (A,B) Kaplan-Meier curves based on TNR (A) and tumor SUVmax (B) for RFS in patients receiving surgery (n=210). (C,D) Kaplan-Meier curves based on TNR (C) and tumor SUVmax (D) for OS in group A (n=278). (E) Kaplan-Meier curves based on TNR and CA19-9 status for OS in patients receiving surgery of group A (n=210). CA19-9–: CA19-9 <37 U/mL; CA19-9+: CA19-9 ≥37 U/mL; TNR–: TNR ≤3.2; TNR+: TNR >3.2. HR, hazard ratio; OS, overall survival; RFS, recurrence-free survival; TNR, tumor-to-non-tumor ratio; SUVmax, maximum standardized uptake value; CA19-9, carbohydrate antigen 19-9.


https://dx.doi.org/10.21037/hbsn-21-25

**Table S4** Univariate and multivariate analyses of prognostic factors of OS in patients receiving surgery (n=210)

| Variables | Univariate P value | I† | | | II‡ | | |
|---|---|---|---|---|---|---|---|
| | | Multivariate | | | Multivariate | | |
| | | HR | 95% CI | P value | HR | 95% CI | P value |
| Age, years (≥63 *vs.* <63) | 0.974 | – | – | NA | – | – | NA |
| Gender (male *vs.* female) | 0.556 | – | – | NA | – | – | NA |
| HBV infection (positive *vs.* negative) | 0.114 | – | – | NA | – | – | NA |
| Clinical symptoms (yes *vs.* no) | 0.008 | – | – | NS | – | – | NS |
| CEA, ng/mL (≥5 *vs.* <5) | 0.001 | – | – | NS | – | – | NS |
| CA19-9, U/mL (≥37 *vs.* <37) | <0.001 | 2.27 | 1.49–3.45 | <0.001 | 2.40 | 1.58–3.64 | <0.001 |
| Liver cirrhosis (yes *vs.* no) | 0.509 | – | – | NA | – | – | NA |
| Tumor size, cm (≥5 *vs.* <5) | 0.052 | – | – | NA | – | – | NS |
| Tumor number (multiple *vs.* single) | <0.001 | 1.97 | 1.35–2.88 | <0.001 | 2.04 | 1.39–2.98 | <0.001 |
| Tumor necrosis (yes *vs.* no) | 0.055 | – | – | NA | – | – | NS |
| Vascular invasion (yes *vs.* no) | 0.002 | – | – | NS | – | – | NS |
| Surrounding tissue invasion (yes *vs.* no) | <0.001 | 1.72 | 1.12–2.65 | 0.013 | 1.71 | 1.11–2.61 | 0.014 |
| Regional LN metastasis (yes *vs.* no) | <0.001 | 2.10 | 1.38–3.20 | <0.001 | 2.11 | 1.39–3.22 | <0.001 |
| Distant metastasis (yes *vs.* no) | <0.001 | 1.77 | 1.02–3.08 | 0.044 | 2.08 | 1.22–3.58 | 0.008 |
| TNR (high *vs.* low) | <0.001 | 1.60 | 1.07–2.38 | 0.023 | – | – | – |
| Tumor SUVmax (high *vs.* low) | 0.002 | – | – | – | – | – | NS |

†, includes clinicopathologic variables and TNR; ‡, includes clinicopathologic variables and tumor SUVmax. OS, overall survival; HR, hazard ratio; CI, confidential interval; CEA, carcinoembryonic antigen; CA19-9, carbohydrate antigen 19-9; LN, lymph node; TNR, tumor-to-non-tumor ratio; SUVmax, maximum standardized uptake value; NA, not applicable; NS, not significant.

**Table S5** Univariate and multivariate analyses of prognostic factors of RFS in patients receiving surgery (n=210)

| Variables | Univariate P value | I† | | | II‡ | | |
|---|---|---|---|---|---|---|---|
| | | Multivariate | | | Multivariate | | |
| | | HR | 95% CI | P value | HR | 95% CI | P value |
| Age, years (≥63 *vs.* <63) | 0.582 | – | – | NA | – | – | NA |
| Gender (male *vs.* female) | 0.952 | – | – | NA | – | – | NA |
| HBV infection (positive *vs.* negative) | 0.942 | – | – | NA | – | – | NA |
| Clinical symptoms (yes *vs.* no) | <0.001 | 1.46 | 1.04–2.04 | 0.028 | 1.52 | 1.08–2.12 | 0.015 |
| CEA, ng/mL (≥5 *vs.* <5) | 0.001 | – | – | NS | – | – | NS |
| CA19-9, U/mL (≥37 *vs.* <37) | 0.029 | – | – | NS | – | – | NS |
| Liver cirrhosis (yes *vs.* no) | 0.390 | – | – | NA | – | – | NA |
| Tumor size, cm (≥5 *vs.* <5) | 0.006 | – | – | NS | – | – | NS |
| Tumor number (multiple *vs.* single) | <0.001 | 1.88 | 1.35–2.61 | <0.001 | 1.94 | 1.39–2.71 | <0.001 |
| Tumor necrosis (yes *vs.* no) | <0.001 | 2.27 | 1.14–2.27 | 0.006 | 1.70 | 1.21–2.39 | 0.002 |
| Vascular invasion (yes *vs.* no) | 0.042 | – | – | NS | – | – | NS |
| Surrounding tissue invasion (yes *vs.* no) | 0.008 | – | – | NS | – | – | NS |
| Regional LN metastasis (yes *vs.* no) | <0.001 | 2.01 | 1.41–2.86 | <0.001 | 1.99 | 1.39–2.85 | <0.001 |
| Distant metastasis (yes *vs.* no) | 0.001 | – | – | NS | – | – | NS |
| TNR (high *vs.* low) | <0.001 | 1.63 | 1.18–2.25 | 0.003 | – | – | – |
| Tumor SUVmax (high *vs.* low) | 0.001 | – | – | – | – | – | NS |

†, includes clinicopathologic variables and TNR; ‡, includes clinicopathologic variables and tumor SUVmax. RFS, recurrence-free survival; HR, hazard ratio; CI, confidential interval; CEA, carcinoembryonic antigen; CA19-9, carbohydrate antigen 19-9; LN, lymph node; TNR, tumor-to-non-tumor ratio; SUVmax, maximum standardized uptake value; NA, not applicable; NS, not significant.


https://dx.doi.org/10.21037/hbsn-21-25

**Table S6** Multivariate analyses of prognostic factors of OS before PSM (n=639)

| Variables | HR | 95% CI | P value[†] |
|---|---|---|---|
| Age, years (≥63 *vs.* <63) | 1.13 | 0.91–1.40 | 0.258 |
| Gender (male *vs.* female) | 0.96 | 0.77–1.20 | 0.734 |
| HBV infection (positive *vs.* negative) | 0.70 | 0.54–0.91 | 0.008 |
| Clinical symptoms (yes *vs.* no) | 1.33 | 1.06–1.66 | 0.014 |
| CEA, ng/mL (≥5 *vs.* <5) | 1.44 | 1.13–1.83 | 0.003 |
| CA19-9, U/mL (≥37 *vs.* <37) | 1.32 | 1.06–1.66 | 0.020 |
| Liver cirrhosis (yes *vs.* no) | 1.19 | 0.88–1.62 | 0.263 |
| Tumor size, cm (≥5 *vs.* <5) | 1.11 | 0.86–1.44 | 0.425 |
| Tumor number (multiple *vs.* single) | 1.87 | 1.47–2.37 | <0.001 |
| Tumor necrosis (yes *vs.* no) | 1.17 | 0.91–1.50 | 0.213 |
| Vascular invasion (yes *vs.* no) | 1.31 | 1.04–1.65 | 0.023 |
| Surrounding tissue invasion (yes *vs.* no) | 1.35 | 1.04–1.74 | 0.023 |
| Regional LN metastasis (yes *vs.* no) | 2.04 | 1.56–2.67 | <0.001 |
| Distant metastasis (yes *vs.* no) | 2.26 | 1.70–3.02 | <0.001 |
| Performing PET/CT (yes *vs.* no) | 0.78 | 0.62–0.97 | 0.028 |

[†], significance is determined by multivariate Cox proportional hazards regression. OS, overall survival; PSM, propensity score matching; HR, hazard ratio; CI, confidential interval; CA19-9, carbohydrate antigen 19-9; CEA, carcinoembryonic antigen; LN, lymph node; PET/CT, positron emission tomography/computed tomography.


https://dx.doi.org/10.21037/hbsn-21-25